Tunable artificial topological Hall effects in van der Waals heterointerfaces

Meri Algarni, Cheng Tan, Guolin Zheng, Sultan Albarakati, Xiangde Zhu, James Partridge, Yanglin Zhu, Lawrence Farrar, Mingliang Tian, Jianhui Zhou, Xiaolin Wang, Zhiqiang Mao, and Lan Wang

Phys. Rev. B **105**, 155407 — Published 11 April 2022

DOI: 10.1103/PhysRevB.105.155407

Tunable artificial topological Hall effects in van der Waals heterointerfaces

Meri Algarni[1,2#], Cheng Tan[1#], Guolin Zheng[1*], Sultan Albarakati[1], Xiangde Zhu[3], James Partridge[1], Yanglin Zhu[6], Lawrence Farrar[1], Mingliang Tian[3,4,5], Jianhui Zhou[3], Xiaolin Wang[7,8], Zhiqiang Mao[6], Lan Wang[1*]

[1]ARC Centre of Excellence in Future Low-Energy Electronics Technologies (FLEET), School of Science, RMIT University, Melbourne, VIC 3001, Australia.

[2]Physics Department, School of Science, Albaha University, Albaha, Alaqiq 4781, Saudi Arabia.

[3]Anhui Province Key Laboratory of Condensed Matter Physics at Extreme Conditions, High Magnetic Field Laboratory, Chinese Academy of Sciences (CAS), Hefei 230031, Anhui, China.

[4]Department of Physics, School of Physics and Materials Science, Anhui University, Hefei 230601, Anhui, China.

[5]Collaborative Innovation Center of Advanced Microstructures, Nanjing University, Nanjing 210093, China.

[6]Department of Physics, Pennsylvania State University, University Park, PA 16802, USA.

[7]ARC Centre for Future Low-Energy Electronics Technologies (FLEET), University of Wollongong, Wollongong, NSW 2500, Australia.

[8]Institute for Superconducting & Electronic Materials, Australian Institute of Innovative Materials, University of Wollongong, Wollongong, NSW 2500, Australia.

[#] Those authors equally contribute to the paper.

[*] Corresponding authors. Correspondence and requests for materials should be addressed to G. Z. (email: guolin.zheng@rmit.edu.au); L. W. (email: lan.wang@rmit.edu.au).

Abstract

The topological Hall effect (THE) originating from a real-space Berry phase is a significant transport signal for chiral spin textures and has been extensively investigated recently due to its potential applications in topological spintronics. Recently, chiral spin textures and THE were realized in heterointerfaces where spacial inversion symmetry (SIS) is naturally broken. However, multi-channel transport in heterointerfaces can mask the intrinsic THE associated with chiral spin textures. Here, we systematically investigate multi-channel transport in two different kinds of van der Waals (vdW) heterointerfaces. In ferromagnetic-ferromagnetic (FM-FM) heterointerfaces with two opposite anomalous Hall effects, multi-channel transport has mimicked both positive and negative THE without involving any topological charges, dubbed as an artificial THE. Moreover, artificial THEs were also observed in FM-metal heterointerfaces consisting of a single FM layer stacked onto a nodal-line semimetal and was attributed to the presence of multi-channel transport as well. Our findings provide an alternative explanation for THE-like features in heterointerfaces. They also reveal exotic multi-channel transport properties in vdW heterointerfaces which could facilitate the development of multifunctional nanodevices based on vdW heterointerfaces.

The anomalous Hall effect (AHE) is an important phenomena in condensed matter physics that usually occurs in systems with broken time-reversal symmetry, such as in magnetic materials [1]. Experimental and theoretical studies have provided a means to understand the AHE by the Berry curvature of electronic bands [2]. In addition to the Berry phase in reciprocal space, it has been established that the real-space Berry phase (e.g., Skyrmion) adopted by conducting electrons can also result in a Hall response-topological Hall effect (THE) [3, 4], as shown in Fig. 1(a), that resembles the AHE dominated by the Berry phase in the reciprocal space. The real-space topology widely exists in chiral spin textures, which have promising applications in topological spintronics. The THE has thus been experimentally employed to detect chiral spin textures in chiral magnets [5-9] or in heterointerfaces with naturally broken SIS [10-16]. Importantly, hybrid Hall effects observed in heterointerfaces usually arise from multi-channel transport which can mask the intrinsic THE associated with chiral spin textures. Further investigation in this area would significantly inspire the study of the associated novel phenomena.

Previous studies have demonstrated that magnetic heterointerfaces prepared by pulsed laser deposition or molecular beam epitaxy can mimic the Skyrmion-like Hall effect due to the competition of two opposite AHEs [17-21]. THE-like signals raised from the film inhomogeneities [22] and multiple magnetotransport channels in multilayers [23, 24] have also been reported recently. The observed Skyrmion-like Hall effect in those heterointerfaces with similar lattice structures usually exhibit only either a “hump” or a “dip” in anomalous Hall loops, as shown in Fig. 1(b). In this article, we demonstrate that the artificially stacked magnetic van der Waals (vdW) heterointerfaces with significantly differing lattice structures and magnetic properties can reproduce both “hump” and “dip” structures in a single anomalous Hall loop, due to the competition of two opposite AHEs. Our magnetic heterointerfaces consist of a ferromagnetic (FM) Fe_3GeTe_2 (FGT) layer with a positive AHE and a FM $Fe_{0.26}TaS_2$ (FTS)

layer with an opposite AHE separated by a thin graphite (Gr) layer. The "hump" structures near the coercivities were observed to evolve into "dip" structures as the temperature was altered. Within a certain temperature range, both "hump" and "dip" structures coexist in a single Hall loop, resembling the respective positive and negative THE observed in a chiral magnetic system [25]. Since the two magnetic layers are decoupled and separated by a graphite layer, the observed "hump" or "dip" features exhibited by the FGT/Gr/FTS heterointerfaces do not involve in any real-space topology. These peak structures were also found to vary with the thicknesses of the FGT and FTS layers, suggesting the potential tunability of the multi-channel transport properties in the vdW heterointerfaces by controlling the layer thicknesses within them. Notably, the "hump" structures in the Hall trace were even reproduced in a FM-metal heterointerface by assembling a single magnetic layer with a two-band metallic layer, as illustrated in Figs. 1(c) and 1(d). The nodal line semimetal ZrSiSe (ZSS) was chosen for these experiments and incorporated into FTS/Gr/ZSS heterointerfaces. The combined Hall trace from the FTS/Gr/ZSS interfaces indeed exhibited "hump" anomalies over a large temperature range, which can be attributed to multi-channel transport as well. Our findings reveal that THE-like features may widely exist in vdW heterointerfaces due to their characteristic multi-channel transport which may not necessarily involve any topological charges or two magnetic layers with opposite AHEs.

We first focus on a FM-FM heterointerface with two opposite AHEs. Fig. 2(a) shows the layout of our device. The device consists of an upper FGT layer and a lower FTS layer separated by a spacer. A graphite layer (around 10 nm) was chosen as the spacer because the Hall response of graphite is almost linear over a large temperature range. Since graphite has a negligible spin-orbit coupling (SOC), it doesn't support a Dzyaloshinskii-Moriya interaction (DMI) and the resultant chiral spin textures at its interfaces. Fig. 2(b) illustrates the AHEs under different temperatures in a typical FGT nanoflake with thickness around 70 nm. FGT is a typical vdW

ferromagnet with large perpendicular magnetic anisotropy and high Curie temperature (around 220 K) [26-28]. As we can see, the AHEs of FGT are proportional to the magnetization curves (see Supplementary data), revealing a positive AHE. Fig. 2(c) demonstrates the AHEs of a typical FTS nanoflake with a thickness of around 90 nm from 30 K to 70 K. FTS is also a ferromagnetic metal but with a much lower Curie temperature of around 100 K and very large coercivities (Supplementary data). In contrast to FGT, the AHEs in FTS oppose the magnetization process (Supplementary data), indicating a negative AHE. It has been reported that both FGT and FTS are dominated by intrinsic AHE at low temperatures [29, 30]. For the intrinsic AHE, the anomalous Hall conductivity is determined by the integration of Berry curvature in reciprocal space [2]. The positive AHE indicates a positive integration and vice-versa. Due to the different coercivities and different Curie temperatures of the layers, the hybrid AHE of FGT/Gr/FTS heterostructures is expected to exhibit interesting phenomena.

Fig. 3 shows the multi-channel Hall effects in FGT/Gr/FTS heterointerfaces. Since FGT and FTS have different coercivities and anomalous Hall resistivities, the trace of hybrid anomalous Hall resistance would strongly depend on the current ratio passing through the two different magnetic layers. For clarity but without loss of generality, we fabricated two FGT/Gr/FTS heterostructure devices with different FGT and FTS thicknesses. In sample #1, the thickness of the FGT was 35 nm while the FTS was 95 nm thick. The two magnetic layers were separated by a graphite spacer (around 10 nm thick). In sample #2, the thicknesses of the FGT and FTS layers were nearly identical (60 nm) while the graphite layer was again 10 nm thick. Fig. 3(a) demonstrates the multi-channel AHEs in sample #1 under different temperatures. Interestingly, the anomalous Hall resistance of FGT R_{xy}^{FGT} is similar in amplitude to R_{xy}^{FTS} between 40 and 50 K. Due to the opposite signs, the combined anomalous Hall resistance R_{xy}^{tot} in sample #1 approaches zero when the magnetic field $B \leq |H_c^{FGT}|$ (with H_c^{FGT} being the coercivity of FGT) in this temperature range. However, extra positive "hump" structures were observed for the

magnetic field $|H_c^{FGT}| \leq B \leq |H_c^{FTS}|$ (H_c^{FTS} is the coercivity of FTS), resembling the positive THE arising from positive topological charges. Note that, due to the dramatic change of H_c^{FTS} with respect to the temperatures, the "hump" structures diminished rapidly as the temperature was increased from 40 K to 49 K. Above 49 K, the amplitude of R_{xy}^{FGT} surpassed the amplitude of R_{xy}^{FTS}, $\left|R_{xy}^{FGT}\right| > \left|R_{xy}^{FTS}\right|$. The combined AHE above 49 K then became positive, as seen in Fig. 3(a). Moreover, both "hump" and "dip" structures were observed in a single Hall loop between 50 K and 52 K, resembling both positive and negative THE induced by topological charges. Further elevating the temperature, the "hump" structures disappeared while the "dip" structures became more intense. Hence, a transformation from "hump" structures at low temperatures to "dip" structures occurred above 52 K. Meanwhile, due to the suppression of R_{xy}^{FTS}, the combined anomalous Hall resistance R_{xy}^{tot} at B=0 T gradually increased. When the temperature exceeded 80 K, ferromagnetism in the FTS layer was suppressed and the AHE of FTS vanished. The combined AHE was then dominated by the contribution from the FGT layer. As shown in Fig. 3(a), the total anomalous Hall loop measured from this heterointerface at 100 K features square-shaped hysteresis that is characteristic of the intrinsic AHE in FGT at this temperature.

If the thicknesses of both FGT and FTS layers are altered, the combined Hall trace can be tuned. Fig. 3(b) shows the two-channel Hall effect of sample #2 (in which both FGT and FTS layers were around 60 nm thickness). With the significant increase in the thickness of the FGT relative to the sample #1, the combined Hall resistance R_{xy}^{tot} in sample #2 should be much larger than that exhibited by sample #1 near B=0 T. Indeed, it can be seen from Fig. 3b that the hybrid AHEs are always positive from 35 K to 52 K. Additionally, the observed "hump" structures do not transform to "dip" structures over that temperature range. These two-channel Hall effects appear to be very similar to previously reported THE [10-16] induced by the large DMI due to the strong SOC and broken SIS at heterointerfaces. However, due to the ignorable SOC in

graphene, the FGT/Gr or Gr/FTS heterointerfaces don't support a nonzero DMI as well as any real space topological spin textures. We conclude that for heterointerfaces that support two opposite AHEs, two-channel transport can indeed mimic both positive and negative THE. This could mask the intrinsic THE associated with chiral spin textures. To distinguish between the two possible origins, careful analysis of the AHEs in the separate magnetic layers should be performed. To further validate the two-channel scenario, we conduct linear regression analysis on the remanences of anomalous Hall traces. Fig. 3c displays the fitting curves for the remanences of device #1 and #2. Note that the remanence discussed here refers to the value of $R_{xy}(B = 0\ \mathrm{T})$ after the magnetic field reduces from saturated fields. Here, two typical remanence curves of FGT [$R_{FGT}^{Rem}(T)$, 40 nm] and FTS [$R_{FTS}^{Rem}(T)$, 80 nm] nanoflakes (see the upper figure of Fig. 3c) were utilized to perform the linear regression analysis. The detailed measurements of the temperature dependent remanence curve were discussed previously [23]. The remanence values of both sample #1 and #2 now conform to $R_{tot}^{Rem} = a + bR_{FTS}^{Rem} + cR_{FGT}^{Rem}$, where $R_{tot}^{Rem}, R_{FGT}^{Rem}, R_{FTS}^{Rem}$ represents the remanence of the heterointerface, FGT and FTS, respectively and the fitting parameters a is a contributing factor from the graphene, it is close to zero due to the paramagnetic characteristic of graphene. b, c are the respective contributing factors of the FTS and FGT, which might depend on the sizes, resistivity and metal electrode contact of each layer. However, the tendency of R_{tot}^{Rem}(T) is almost the same in device #1 and device #2. As we can see in the lower two figures of Fig. 3c, the remanences of device #1 and device #2 can be well-fitted by the liner superposition of remanence from FGT and FTS layers, which further supports the multi-channel transport scenario. Note that, the resistivities of FTS, graphite and FGT are quite different which might lead to an inhomogeneous distribution of current in each layer. Since FGT has higher resistivity, we put it on top of the heterostructures to ensure that enough current could flow through FGT and generate sizable AHE signals in both FGT and FTS layers. Despite the different resistivities in each layer, however, these discrepancies are

almost unchanged in our fitting temperature range (typically between 40 K and 80 K) which validates the fittings in Fig. 3.

Besides the two-AHE scenario, we found that a single magnetic layer stacked onto a two-band nodal-line semimetal (ZrSiSe) also generated a skyrmion-like Hall trace, as illustrated in Figs 1c and 1d. It is well-established that ZrSiSe is a two-band Dirac semimetal with a "nonlinear" Hall trace [31] resembling an AHE without hysteresis. Supplementary Fig. 3 shows the Hall resistances of a typical ZrSiSe nanoflake at different temperatures. Fig. 4 shows the two-channel transport properties in one of our FTS/Gr/ZSS devices with layer thicknesses 70 nm (FTS), around 10 nm (Gr) and 110 nm (ZSS). The solid black curve in Fig. 4a shows the total Hall resistance at 20 K, which, at first glance contains a linear ordinary Hall contribution (dashed linear curve) and extra "hump" structures near the coercivities (shaded light yellow). However, this "hump" structure merely originates from the two-band character of ZrSiSe, and the corresponding two-band Hall component is shown by the blue curve in Fig. 4a. The linear ordinary Hall contribution is subtracted to reveal the Hall component ΔR_{xy} at different temperatures, as shown in Fig. 4b. Due to the two-band character of Dirac semimetal ZrSiSe, the hybrid Hall effect in FTS/Gr/ZSS heterointerface also exhibits "hump" features which resemble Skyrmion-like THE. This multi-channel transport in artificial FM-metal heterointerfaces has been overlooked so far and as a result, similar "hump" features observed in Hall traces might be mistakenly attributed to THE raised by chiral spin textures. Our experiments therefore provide an alternative explanation for unconventional AHEs that may be observed in a variety of heterointerfaces.

In conclusion, we systematically studied the multi-channel Hall effects in different kinds of van der Waals heterointerfaces. We unveiled both "hump" and "dip" structures near the coercivities in anomalous Hall loops in FM/Gr/FM heterointerfaces with two opposite AHEs and the "hump" features in FM/Gr/metal heterointerface even without the two opposite AHEs.

These features, resembling Skyrmion-like THE in chiral magnets, can be well captured by multi-channel transport without involving any chiral spin textures. Our findings advance the understanding of the multi-channel transport properties in artificial heterointerfaces.

ACKNOWLEDGEMENTS

The work at RMIT was supported by the Australian Research Council Centre of Excellence in Future Low-Energy Electronics Technologies (Project No. CE170100039). The crystal growth efforts of ZiSiSe was supported by the US Department of Energy under grants DE-SC0019068.

Figure captions

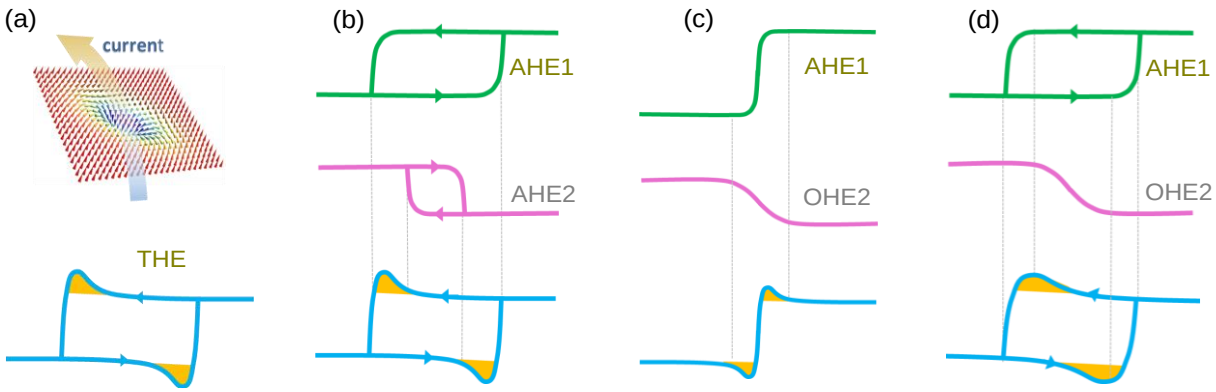

FIG 1. Possible origins of Skyrmion-like Hall effects. (a) An intrinsic topological Hall effect in chiral magnets. (b) Hybrid anomalous Hall effect in a heterointerface constructed with two decoupled magnetic layers with opposite signs. (c) and (d) Two-channel Hall effects in a FM-metal heterointerface. The metallic layer is a two-band metal with a nonlinear, ordinary Hall effect (OHE). The FM layer might exhibit no hysteresis (c) or a large hysteresis loop (d).

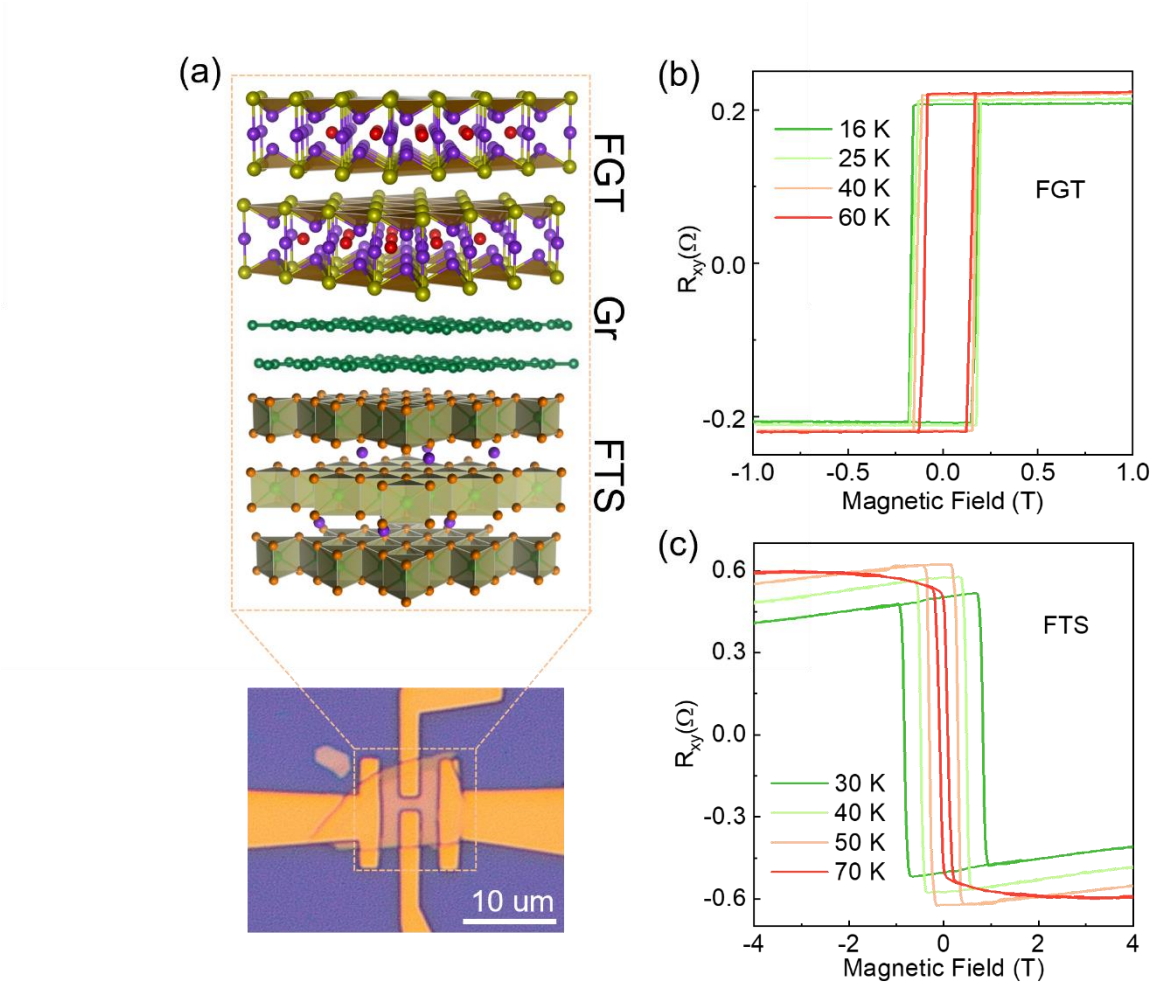

FIG 2. Device structure and anomalous Hall effects in FGT and FTS. (a) The structure of the FGT/Gr/FTS heterostructure device. (b) shows positive AHEs in a typical FGT nanoflake in the temperature range 16-60 K. Due to the strong FM order and high Curie temperature of FGT, both coercivities and anomalous Hall resistances are relatively unchanged in this temperature range. (c) shows negative AHEs in a typical FTS nanoflake in the temperature range 30-70 K. In sharp contrast to AHEs in FGT, both coercivities and anomalous Hall resistances changed dramatically with the increase of temperature.

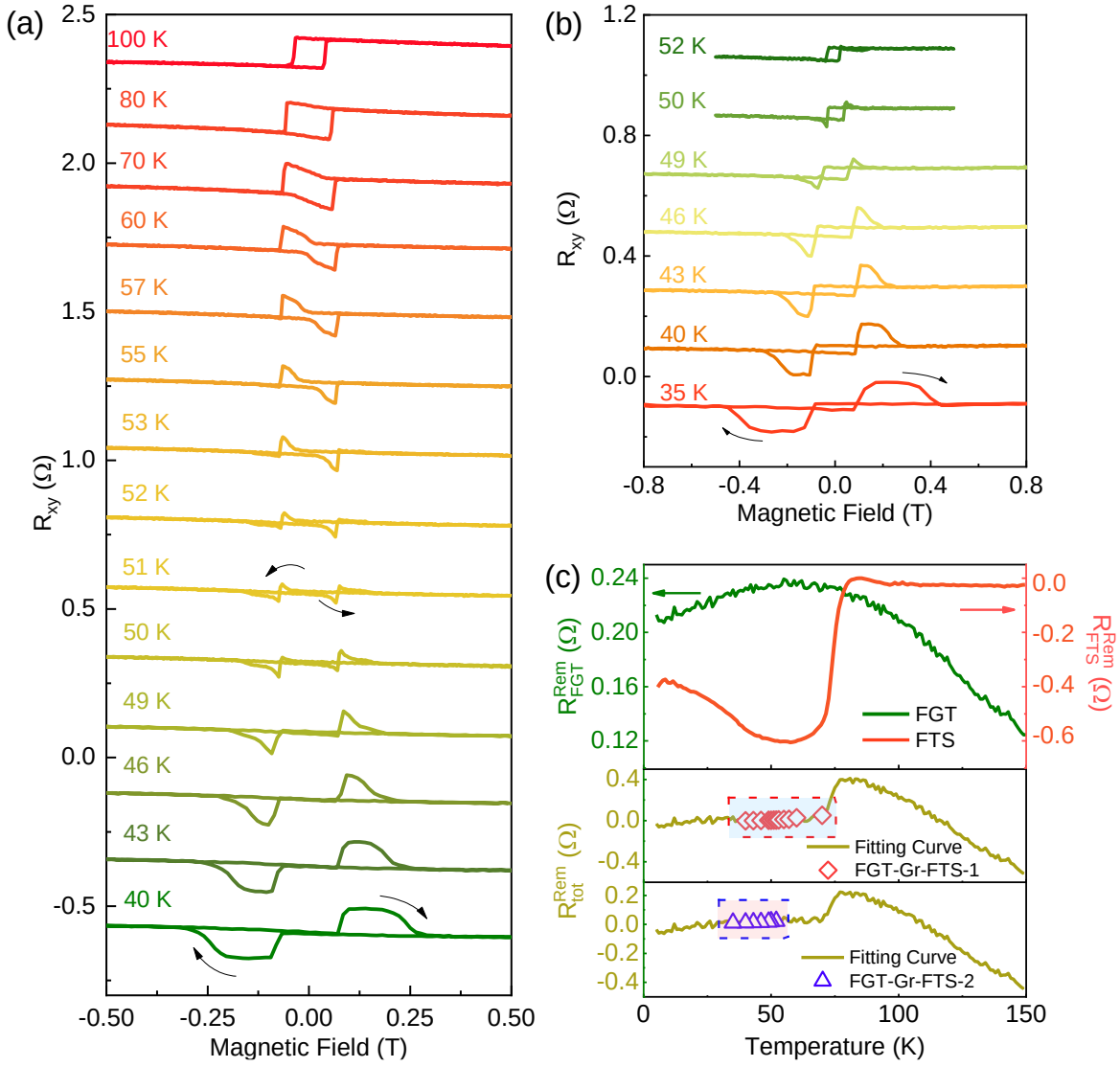

FIG 3. Multi-channel anomalous Hall effect in FGT/Gr/FTS heterointerfaces and the remanence fitting. (a) The multi-channel AHE in sample #1 with the thickness of the FTS layer (95 nm) significantly exceeding that of the FGT layer. The two-channel transport shows that $\left|R_{xy}^{FGT}\right|$ equals $\left|R_{xy}^{FTS}\right|$, causing R_{xy}^{total} to vanish at B = 0 T between 40 K and 46 K. (b) The multi-channel transport in sample #2. Increasing the anomalous Hall contribution of the FGT layer (both FTS layer and FGT layer are 60 nm thick in sample #2), ensures that the hybrid anomalous Hall effects are always positive. Both samples exhibit Skyrmion-like "hump" or "dip" features in their Hall traces. All Hall traces are vertically shifted for clarity. (c) Linear regression analysis of the remanences in device #1 (FGT-Gr-FTS-1) and device 2 (FGT-Gr-FTS-2). Two typical

remanence curves of FGT (red, 40 nm) and FTS (green, 80 nm) were utilized to linearly fit the remanence of device #1 and #2.

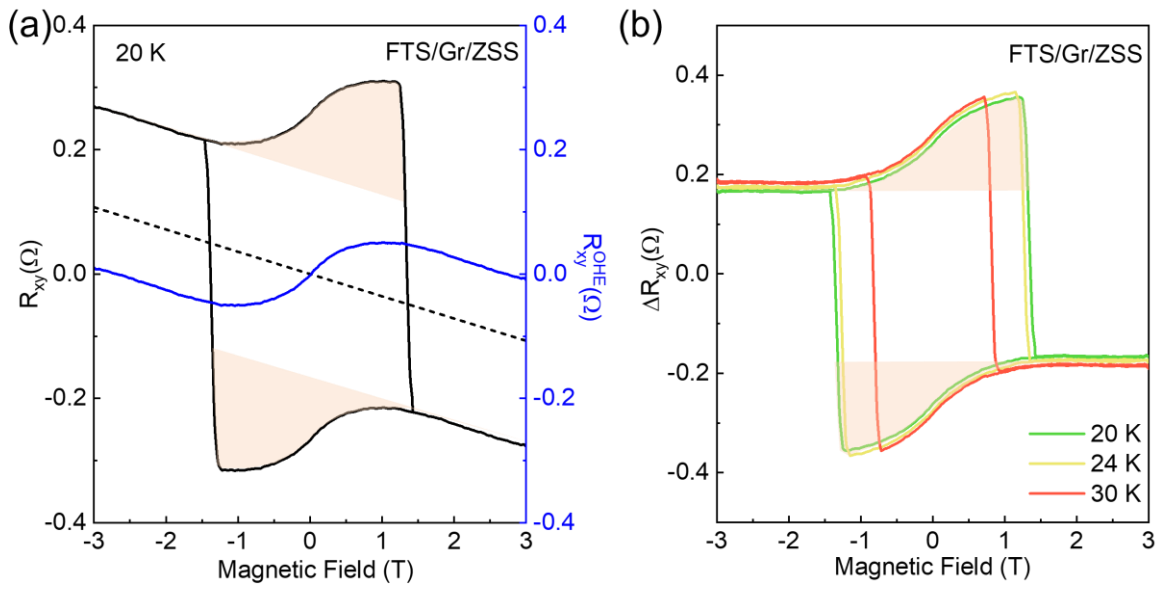

FIG 4. Multi-channel transport in FTS/Gr/ZSS heterointerfaces. (a) the hybrid Hall effect in a typical FTS/Gr/ZSS sample at 20 K (black curve). Due to the two-band character of ZrSiSe, the hybrid Hall resistance contains a "hump" structure (shaded light yellow) and a linear Hall contribution (dashed line). The blue curve indicates the possible two-band Hall component of ZrSiSe after subtracting the anomalous Hall part (light blue part). (b) shows the hybrid Hall component ΔR_{xy} at different temperatures after subtracting the linear Hall contribution.

REFERENCES

[1] E. Hall, On the Possibility of Transvers Currents in Ferromagnets, Philos. Mag. **12,** 157 (1881).

[2] N. Nagaosa, J. Sinova, S. Onoda, A. H. MacDonald and N. P. Ong, Anomalous Hall Effect, Rev. Mod. Phys. **82,** 1539 (2010).

[3] J. Ye, Y. B. Kim, A. Millis, B. Shraiman, P. Majumdar and Z. Tešanović, Berry Phase Theory of the Anomalous Hall Effect: Application to Colossal Magnetoresistance Manganites. Phys. Rev. Lett. **83,** 3737 (1999).

[4] P. Bruno, V. Dugaev and M. Taillefumier, Topological Hall Effect and Berry Phase in Magnetic Nanostructures, Phys. Rev. Lett. **93,** 096806 (2004).

[5] A. Neubauer, C. Pfleiderer, B, Binz, A. Rosch, R. Ritz, P. Niklowitz and P. Böni, Topological Hall Effect in the A Phase of MnSi, Phys. Rev. Lett. **102,** 186602 (2009).

[6] N. Kanazawa, Y. Onose, T. Arima, D. Okuyama, K. Ohoyama, S. Wakimoto, K. Kakurai, S. Ishiwata and Y. Tokura, Large Topological Hall Effect in a Short-Period Helimagnet MnGe. Phys. Rev. Lett. **106,** 156603 (2011).

[7] Y. Li, N. Kanazawa, X. Z. Yu, A. Tsukazaki, M. Kawasaki, M. Ichikawa, X. Jin, F. Kagawa and Y. Tokura, Robust Formation of Skyrmions and Topological Hall Effect Anomaly in Epitaxial Thin Films of MnSi, Phys. Rev. Lett. **110,** 117202 (2013).

[8] C. Franz, C. Freimuth, F. Bauer, A. Ritz, R. Schnarr, C. Duvinage, C. Adams, T. Blügel, S. Rosch, A. Mokrousov and C. Pfleiderer, Real-Space and Reciprocal-Space Berry Phases in the Hall Effect of $Mn_{1-x}Fe_xSi$, Phys. Rev. Lett. **112,** 186601 (2014).

[9] D. Liang, J. P. DeGrave, M. J. Stolt, Y.Tokura and S. Jin, Current-Driven Dynamics of Skyrmions Stabilized in MnSi Nanowires Revealed by Topological Hall Effect, Nat. Commun. **6,** 8217 (2015).

[10] K. Yasuda, R. Wakatsuki, T. Morimoto, R. Yoshimi, A. Tsukazaki, K. Takahashi, M. Ezawa, M. Kawasaki, N. Nagaosa and Y. Tokura, Hall Effects in Topological Insulator Heterostructures, Nat. Phys. **12,** 555 (2016).

[11] J. Matsuno, N. Ogawa, K.Yasuda, F. Kagawa, W. Koshibae, N. Nagaosa, Y. Tokura and M. Kawasaki, Interface-Driven Topological Hall Effect in $SrRuO_3$-$SrIrO_3$ Bilayer, Sci. Adv. **2,** e1600304 (2016).

[12] C. Liu, Y. Zang, W. Ruan, Y. Gong, K. He, X. Ma, Q.-K. Xue, and Y. Wang, Dimensional Crossover-Induced Topological Hall Effect in a Magnetic Topological Insulator, Phys. Rev. Lett. **119,** 176809 (2017).

[13] Y. Ohuchi, J. Matsuno, N. Ogawa, Y. Kozuka, M. Uchida, Y. Tokura and M. Kawasaki, Electric-Field Control of Anomalous and Topological Hall Effects in Oxide Bilayer Thin Films, Nat. Commun. **9,** 213 (2018).

[14] Q. L. He, G. Yin, A. J. Grutter, L. Pan, X. Che, G. Yu, D. A. Gilbert, S. M. Disseler, Y. Liu, P. Shafer, B. Zhang, Y. Wu, B. J. Kirby, E. Arenholz, R. K. Lake, X. Han and K. L. Wang, Exchange-Biasing Topological Charges by Antiferromagnetism, Nat. Commun. **9,** 2767 (2018).

[15] M. Raju, A. Yagil, A. Soumyanarayanan, A. K. Tan, A. Almoalem, F. Ma, O. Auslaender and C. Panagopoulos, The Evolution of Skyrmions in Ir/Fe/Co/Pt Multilayers and Their Topological Hall Signature, Nat. Commun. **10,** 696 (2019).

[16] J. Jiang, D. Xiao, F. Wang, J.-H. Shin, D. Andreoli, J. Zhang, R. Xiao, Y.-F. Zhao, M. Kayyalha, L. Zhang, K. Wang, J. Zang, C. Liu, N. Samarth, M. H. W. Chan and C.-Z. Chang, Concurrence of Quantum Anomalous Hall and Topological Hall Effects in Magnetic Topological Insulator Sandwich Heterostructures, *Nat. Mater.* **19,** 732 (2020).

[17] D. J. Groenendijk, C. Autieri, T. C. van Thiel, W. Brzezicki, J. Hortensius, D. Afanasiev, N. Gauquelin, P. Barone, K. van den Bos, S. van Aert, J. Verbeeck, A. Filippetti, S. Picozzi, M. Cuoco and A. D. Caviglia, Berry Phase Engineering at Oxide Interfaces, Phys. Rev. Research **2,** 023404 (2020).

[18] D. Zheng, Y.-W. Fang, S. Zhang, P. Li, Y. Wen, B. Fang, X. He, Y. Li, C. Zhang, W. Tong, W. Mi, H. Bai, H. N. Alshareef, Z. Q. Qiu and X. Zhang, Berry Phase Engineering in $SrRuO_3$/$SrIrO_3$/$SrTiO_3$ Superlattices Induced by Band Structure Reconstruction, ACS Nano **15,** 5086 (2021).

[19] K. M. Fijalkowski, M. Hartl, M. Winnerlein, P. Mandal, S. Schreyeck, K. Brunner, C. Gould and L. W. Molenkamp, Coexistence of Surface and Bulk Ferromagnetism Mimics Skyrmion Hall Effect in a Topological Insulator, Phys. Rev. X **10,** 011012 (2020).

[20] P. Chen, Y. Zhang, Q. Yao, F. Tian, L. Li, Z. Qi, X. Liu, L. Liao, C. Song, J. Wang, G. Li, D. M. Burn, G. van der Laan, T. Hesjedal, S. Zhang and X. Kou, Tailoring the Hybrid Anomalous Hall Response in Engineered Magnetic Topological Insulator Heterostructures, Nano Lett. **20,** 1731 (2020).

[21] F. Wang, X. Wang, Y.-F. Zhao, D. Xiao, L.-J. Zhou, W. Liu, Z. Zhang, W. Zhao, M. H. W. Chan, N. Samarth, C. Liu, H. Zhang and C.-Z. Chang, Interface-Induced Sign Reversal of the Anomalous Hall Effect in Magnetic Topological Insulator Heterostructures, Nat. Commun. **12,** 79 (2021).

[22] D. Kan, T. Moriyama, K. Kobayashi and Y. Shimakawa, Alternative to the Topological Interpretation of the Transverse Resistivity Anomalies in $SrRuO_3$, Phys. Rev. B **98,** 180408 (2018).

[23] A. Gerber, Interpretation of Experimental Evidence of the Topological Hall Effect, Phys. Rev. B **98,** 214440 (2018).

[24] L. Yang, L. Wysocki, J. Schöpf, L. Jin, A. Kovács, F. Gunkel, R. Dittmann, P. H. M. van Loosdrecht and I. Lindfors-Vrejoiu, Origin of the Hump Anomalies in the Hall Resistance Loops of Ultrathin $SrRuO_3$/$SrIrO_3$ Multilayers, Phys. Rev. Mater. **5,** 014403 (2021).

[25] W. Wang, Y.-F. Zhao, F. Wang, M. W. Daniels, C.-Z. Chang, J. Zang, D. Xiao and W. Wu, Chiral-Bubble-Induced Topological Hall Effect in Ferromagnetic Topological Insulator Heterostructures, Nano Lett. **21,** 1108 (2021).

[26] C. Tan, J. Lee, S.-G. Jung, T. Park, S. Albarakati, J. Partridge, M. R. Field, D. G. McCulloch, L. Wang and C. Lee, Hard Magnetic Properties in Nanoflake van der Waals Fe_3GeTe_2, Nat. Commun. **9,** 1554 (2018).

[27] S. Albarakati, C. Tan, Z.-J. Chen, J. G. Partridge, G. Zheng, L. Farrar, E. L. Mayes, M. R. Field, C. Lee, Y. Wang, Y. Xiong, M. Tian, F. Xiang, A. R. Hamilton, O. A. Tretiakov, D. Culcer, Y-J. Zhao and L. Wang, Antisymmetric Magnetoresistance in van der Waals Fe_3GeTe_2/graphite/Fe_3GeTe_2 trilayer heterostructures, Sci. Adv. **5,** eaaw0409 (2019).

[28] G. Zheng, W.-Q. Xie, S. Albarakati, M. Algarni, C. Tan, Y. Wang, J. Peng, J. Partridge, L. Farrar, J. Yi, Y. Xiong, M. Tian, Y.-J. Zhao and L. Wang, Gate-Tuned Interlayer Coupling in van der Waals Ferromagnet Fe_3GeTe_2 Nanoflakes, Phys. Rev. Lett. **125,** 047202 (2020).

[29] K. Kim,J. Seo, E. Lee, K.-T. Ko, B. Kim, B. G. Jang, J. M. Ok, J. Lee, Y. J. Jo, W. Kang, J. H. Shim, C. Kim, H. W. Yeom, B. I. Min, B.-J. Yang and J. S. Kim, Large Anomalous Hall Current Induced by Topological Nodal Lines in a Ferromagnetic van der Waals Semimetal, Nat. Mater. **17,** 794 (2018).

[30] J. Checkelsky, M. Lee, E. Morosan, R. Cava and N. Ong, Anomalous Hall Effect and Magnetoresistance in the Layered Ferromagnet $Fe_{1/4}TaS_2$: The Inelastic Regime, Phys. Rev. B **77,** 014433 (2008).

[31] J. Hu, Z. Tang, J. Liu, X. Liu, Y. Zhu, D. Graf, K. Myhro, S. Tran, C. N. Lau, J. Wei and Z. Mao, Evidence of Topological Nodal-Line Fermions in ZrSiSe and ZrSiTe, Phys. Rev. Lett. **117,** 016602 (2016).

APPENDIX

1. Methods

Single Crystal Growth

Fe_3GeTe_2 single crystals were purchased from HQ graphene. $Fe_{0.26}TaS_2$ crystals were grown by the chemical vapor transport method with iodine as the transport agent. First, granular Fe, Ta powder and S sponges with mole ratio of 0.26:1:2 were mixed and sealed in an evacuated quartz tube. The tube was heated at 1173 K for one week. Second, the powder obtained and 120 mg iodine were sealed in an evacuated quartz tube with 15mm inner diameter and 18 cm length. The tube was then placed in a horizontal two-zone furnace with the source zone kept at 1223 K and the growth zone kept at 1123 K for 10 days. The as-grown crystals were cleaned in ethanol under ultrasonic agitation. The ZrSiSe single crystals were prepared using a chemical vapor transport method as described in Ref. [28]

Device Fabrication and Transport Measurements

All nanoflakes, including $Fe_{0.26}TaS_2$, Fe_3GeTe_2 and ZrSiSe, were mechanically exfoliated from bulk crystals in a glove box filled with high purity Ar gas with O_2 < 0.1 ppm, H_2O < 0.1 ppm. Nanoflakes with suitable thicknesses were then dry transferred using a polymer-based dry transfer technique. Note that FGT and FTS nanoflakes with smooth surfaces were chosen to construct FTS/FGT heterostructure. Afterwards, the polymer was dissolved in chloroform. Hall-bar structures were fabricated by standard electron-beam lithography (EBL) methods followed by Cr/Au (10 nm/100nm) evaporation in a high vacuum sputtering system with a base pressure less than $10^{-8}\,Torr$. Transport measurements were performed using the electric transport option in a commercial Magnetic Property Measurement System (Quantum Design, MPMS3).

2. Characterization of Fe_3GeTe_2, $Fe_{0.26}TaS_2$ and ZrSiSe

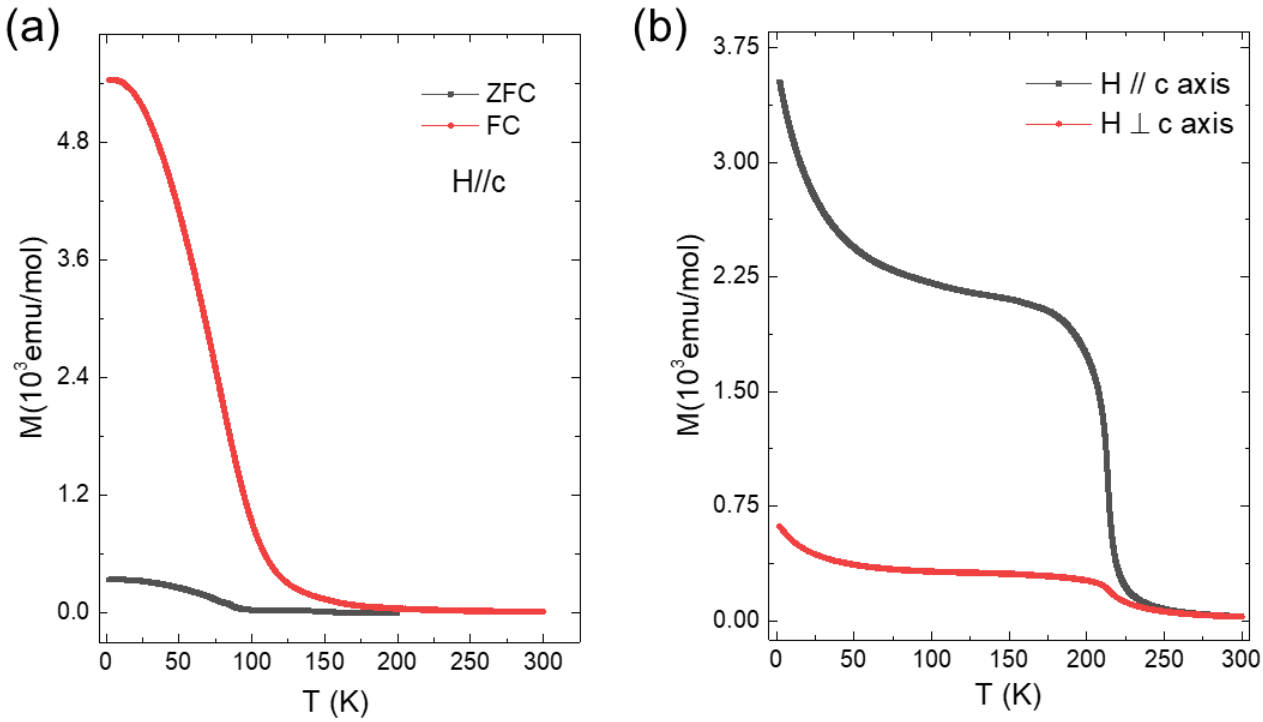

Fig. A1 Temperature-dependent magnetization (M-T) in $Fe_{0.26}TaS_2$ and Fe_3GeTe_2 single crystals. (a) Field cooling (FC, 1T) and zero field cooling (ZFC) M-T curves in single crystal $Fe_{0.26}TaS_2$. From the MT curves, we can get the Curie temperature of $Fe_{0.26}TaS_2$ which is around Tc=100 K. (b) M-T curves in a single crystal Fe_3GeTe_2 with different magnetic field directions with cooling field B=500 Oe. As we can see from M-T curves, the Curie temperature of Fe_3GeTe_2 is around 220 K, much higher than that of $Fe_{0.26}TaS_2$.

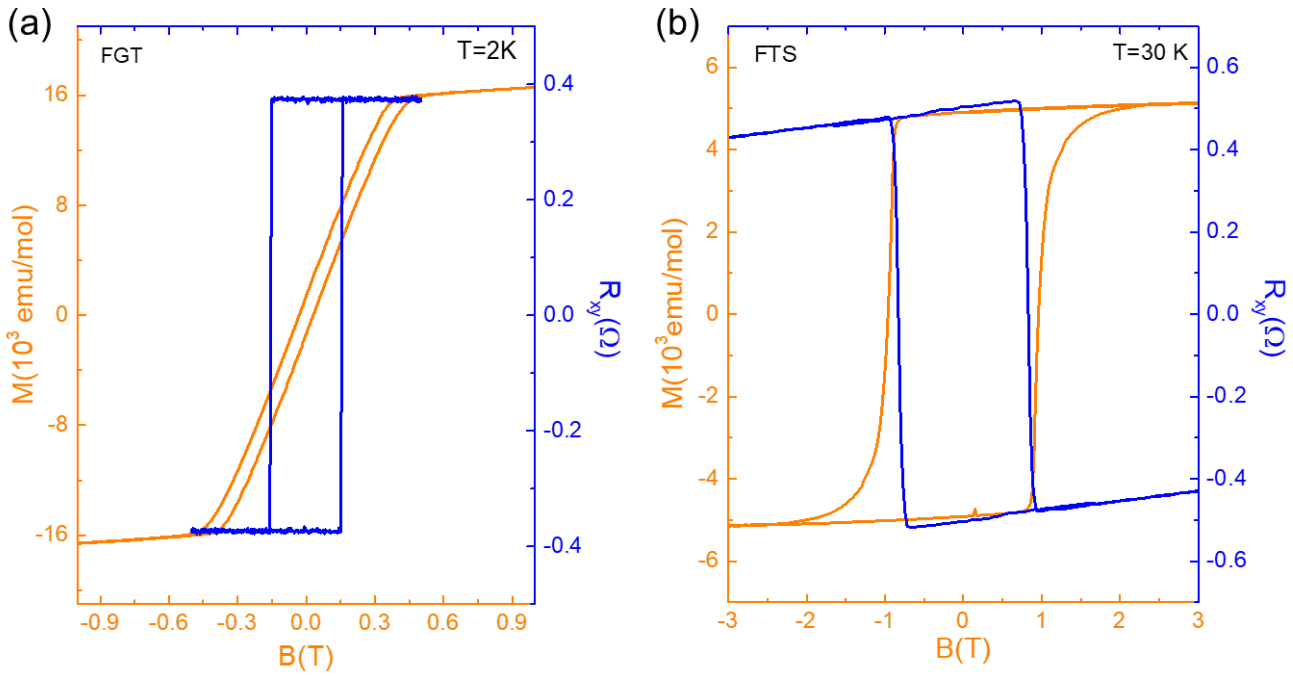

Fig. A2 A comparison between field dependent magnetization (M-H) and anomalous Hall effects in $Fe_{0.26}TaS_2$ and Fe_3GeTe_2. (a) M-H curve in FGT single crystal (orange) and anomalous Hall effect in FGT nanoflake (blue) at 2 K. Note that, the M-H loop is different from the AHE loop, this is because in bulk FGT, the motion of multi-domain will cause a gradual magnetization under magnetic field, while in FGT nanoflake, single domain will dominate and the anomalous Hall usually exhibits a square-shape loop. However, both M-H and AHE exhibit similar tendency, revealing a positive AHE in FGT. (b) M-H curve in FTS single crystal (orange) and anomalous Hall effect in FTS nanoflake (blue) at 30 K. Sharp contrast to FGT, the AHE in FTS is opposite to M-H curve, indicating a negative AHE.

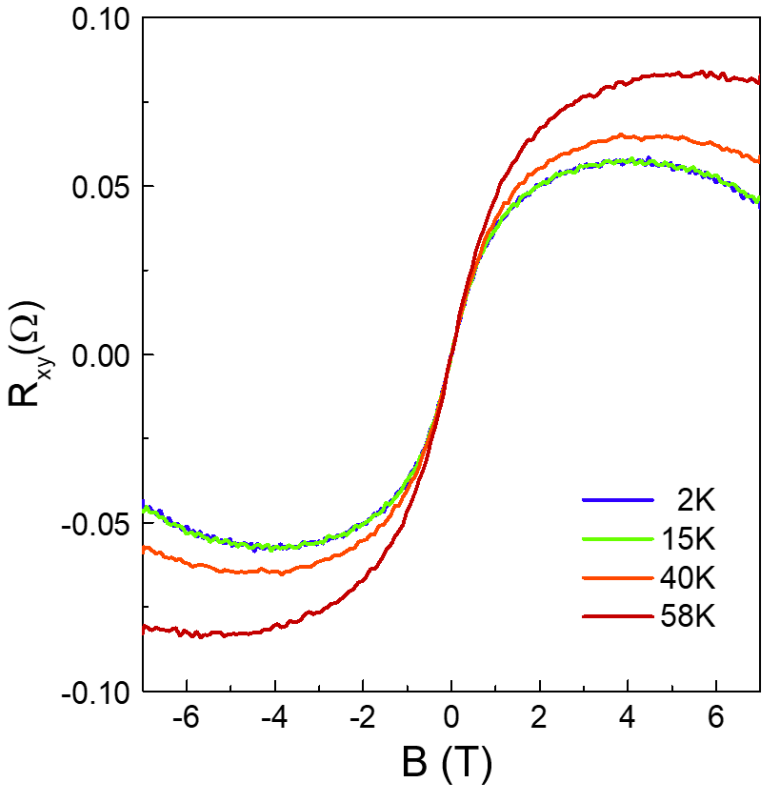

Fig. A3 Hall effects in a typical ZrSiSe nanoflake at different temperatures. As we can see, the Hall effects in Dirac semimetal ZrSiSe exhibit a two-band character, resembling the anomalous Hall resistance without hysteresis.